Collagen polarization provides a structural memory for the elongation of epithelial anlage.

Hiroko Katsuno-Kambe[1], Jessica L. Teo[1], Robert J. Ju[1], James E. Hudson[2], Samantha J. Stehbens[1] and Alpha S. Yap[1,3]

[1]Division of Cell and Developmental Biology, Institute for Molecular Bioscience, The University of Queensland; and
[2]QIMR Berghofer Medical Research Institute, Brisbane, Australia

[3]Correspondence: a.yap@uq.edu.au

Keywords: Epithelia, elongation, tubulogenesis, collagen I, symmetry breaking, anisotropy

Abstract

Branched epithelial networks are fundamental features of many organs in the body. The biogenesis of these networks involves distinct processes where multicellular aggregates elongate and branch. In this report we focus on understanding how the extracellular matrix contributes to the process of elongation. Using mammary epithelial organotypic cultures we found that collagen 1, but not a basement membrane extract, induces the formation of elongated multicellular aggregates. Indeed, isotropic aggregates, used as models of epithelial anlage, broke symmetry and elongated when transplanted into collagen 1 gels; this was accompanied by reorganization of collagen fibrils into bundles that were polarized around the elongating aggregates. By applying external stretch as a cell-independent way to reorganize the ECM gels, we found that collagen polarization itself can induce and guide the direction of aggregate elongation. This critically involves cell proliferation, which is selectively enhanced in the regions of anlage that elongate, and requires β1-integrin and ERK signaling. We propose that collagen polarization promotes anlage elongation by providing a structural memory of the initial axis that is generated when aggregates break symmetry.

Introduction

Branched tubules represent one of the archetypal modes of epithelial organization (Iruela-Arispe and Beitel, 2013; Varner and Nelson, 2014). In organs such as the mammary and salivary glands, lung and kidneys networks of hollow epithelial tubes mediate the physiological exchange of gases, nutrients and solutes between the body and its external environment (Chung and Andrew, 2008). These definitive networks are established by a complex morphogenetic process, where tubules grow outwards from their precursors until they are instructed to branch, after which

outgrowth continues until the network is completed (Affolter et al., 2009; Andrew and Ewald, 2010). The branching and elongation of multicellular aggregates can thus be considered as fundamental processes in the generation of tubular networks.

Interestingly, different organs also use distinct strategies for tubulogenesis. For example, in the trachea, lumens appear early and accompany the growth of tubules (Schottenfeld et al., 2010), whereas in the salivary and mammary glands tubules first begin as non-polarized cellular aggregates (or anlage), which then elongate as solid, multicellular cords before eventually forming lumens (Bastidas-Ponce et al., 2017; Nerger and Nelson, 2018; Tucker, 2007). In the present study we use the mammary epithelium as a model to analyse what guides the elongation of multicellular anlage.

Tubulogenesis is a regulated process. The decision to branch is recognized to be a critical checkpoint that is controlled by developmental signaling. But the elongation of tubule precursors is also thought to be controlled by receptor tyrosine kinases and other signaling pathways (Costantini and Kopan, 2010; Gjorevski and Nelson, 2010; Sternlicht et al., 2006). However, elongation occurs over hours to days, time scales that are much longer than the underlying cellular processes, and the signaling pathways that guide them. This raises the question of whether there may be mechanisms that can help guide elongation over longer time-scales, effectively serving as a bridge between the rapidity of cell signaling and the slow progression of macroscopic anlage elongation. In this study, we show that the extracellular matrix (ECM) represents such a bridge by providing a structural memory for elongation.

The ECM comprises complex mixtures of proteins, glycosaminoglycan and glycoconjugates, which fill the extracellular spaces of tissues and organs (Frantz et al., 2010). One of the main components of ECM is collagen, particularly type 1 collagen (also called collagen 1), which is often the dominant form during epithelial tubulogenesis (Graham et al., 1988; Keely et al., 1995; Llacua et al., 2018; Nakanishi et al., 1986; Simon-Assmann et al., 1995). Notably, fibrillar collagen also helps scaffold other molecules, such other ECM proteins and growth factors (Kanematsu et al., 2004; Wipff and Hinz, 2008). Adhesion between cells and ECM allows the chemical and mechanical properties of the ECM to regulate cell signaling and gene regulation (Shi et al., 2011). Those cell-ECM adhesions also allow cell-based forces to reorganize the ECM. In particular, cells can rearrange collagen fibrils to influence cell migration (Buchmann et al., 2019; Gjorevski et al., 2015; Guo et al., 2012; Shi et al., 2014).

Importantly, fibrillar components of the ECM, such as collagen 1, are relatively long-lived (Price and Spiro, 1977; Verzijl et al., 2000), making them attractive candidates to bridge time scales during tubulogenesis. Indeed, rearrangement of collagen has been implicated in patterning epithelial branching (Brownfield et al., 2013; Guo et al., 2012; Harunaga et al., 2011; Ingman et al., 2006; Patel et al., 2006). However, it is difficult to elucidate the specific contribution for collagen in the complex environment of an organ, where there are many additional contributions from other cell types and various chemotactic signals. Therefore, in this study we used three-dimensional (3D) organotypic cultures to specifically test a role for the

extracellular matrix (ECM). We report that a collagen 1 matrix induces the elongation of mammary epithelial anlage. This is accompanied by the polarization of the matrix itself, an event that sustains anlagen elongation by stimulating cell proliferation.

Results

3D collagen I hydrogels cause mammary epithelial aggregates to break symmetry.

We used 3D cultures of the non-tumorigenic human MCF10A mammary epithelial cell line to test how the ECM influences anlage elongation. Commonly, 3D culture systems are used to study early events that start from single isolated cells. However, for our purposes we developed a system that would allow us to visualize how elongation occurred from a multicellular source. We did this by manipulating the ECM environment in which the cells were grown. When MCF10A cells are grown on Matrigel™ substrates and in media supplemented with soluble Matrigel™ (Debnath et al., 2003), they proliferate from single isolated cells to form a multicellular aggregate, which then polarizes and clears the central mass of apoptotic cells, to generate a central lumen in a process known as cavitation (Fig S1A). In contrast, when isolated cells were embedded in a gel of Type 1 collagen, which is the major ECM component in the stromal environment during mammary tubulogenesis (Schedin and Keely, 2011), they proliferated to form elongated, solid cords of non-polarized cells (Fig S1B) (Krause et al., 2008). This indicated that MCF10A cells provided a useful model of mammary anlage elongation and further suggested that some properties of the collagen 1 environment might provide an instructive cue for elongation.

In order to capture the process by which isotropic aggregates broke symmetry and then elongated, cells were first seeded in Matrigel™ until proliferation arrested at 10 days (Fig 1A); aggregates were then isolated and embedded into collagen (acid solubilized Rat Type I collagen, 37□ for 30 minutes). Lumens were apparent in some Matrigel-embedded aggregates, but most remained as solid spheres, resembling anlage. Consistent with the change in matrix environment, re-embedded aggregates lost laminin V expression over time (Fig S1C). Live-cell imaging revealed that the transplanted aggregates displayed small jiggling motions for several hours, then spontaneously broke symmetry and elongated to form cord-like structures similar to those formed when cultured *de novo* in collagen (Fig 1B and Movie S1). These elongating aggregates were generally solid, with no evident lumens (Fig 2A). Commonly, elongation began with a group of cells that protruded away from the more spherical original aggregate (Fig 1C,E). This confirmed that a collagen I matrix could induce epithelial elongation without any other changes in the culture conditions. We therefore used transplantation into collagen as an assay to examine how this specific ECM environment could induce and sustain anlagen elongation.

Cell proliferation drives anlagen elongation

Multiple cellular processes have been implicated in epithelial elongation, notably cell migration, as well as polarization and proliferation (Andrew and Ewald, 2010; Economou et al., 2013; Keller, 2002). However, tracking of cell nuclei showed that cells moved with the same speed in the elongating parts of an aggregate as in the non-elongating parts (Fig S2). This suggested that, while migration may be necessary for elongation, regional variations in migration speed did not drive elongation.

We then focused on cell proliferation by staining for Ki-67 (Fig 1C,D), a nonhistone nuclear protein commonly used as a marker of proliferating cells in mammalian cells (Soliman and Yussif, 2016). Ki-67 staining was evident when aggregates were examined 8 d after transfer into collagen 1. Strikingly, Ki-67-positive cells were more frequent in the elongating areas (41.00 ± 4.55 % of all cells) compared with the non-elongating areas (18.86 ± 3.05 %) (Fig 1 C,D). Live-cell imaging of cells expressing NLS-mCherry also showed that the proportion of nuclei that divided was higher in the elongating than the non-elongating areas (Fig 1D-F).

Importantly, elongation was inhibited when we blocked proliferation using the cell cycle inhibitors mitomycin C and aphidicolin (Fig 1H). Control cultures progressively increased their proportion of Ki-67-positive cells after transplantation into collagen (from 2.28 ± 0.85 % at Day 1 to 26.63 ± 3.34 % at Day 8). However, cell proliferation was significantly reduced by mitomycin C (3.88 ± 1.18 %, Day 8) and aphidicolin (11.54 ± 3.55 %, Day 8) (Fig 1I). Aggregate elongation was also significantly reduced by both mitotic inhibitors (Fig 1J). To quantitate this, we calculated a symmetry ratio, i.e., the ratio of the maximum length (L_1) and width (L_2) of the aggregates. Completely round aggregates will have a symmetry ratio of 1, whereas for elongated aggregates L_1/L_2 will be >1 (Fig 2B). The symmetry ratio increased as control anlage elongated, and this was blocked by both mitomycin C and aphidicolin (Fig 1J). Thus, cell proliferation triggered by collagen 1 was a key driver of epithelial elongation, whose inhibition was not compensated for by other processes, such as cell migration.

Cells within the elongating regions also tended to divide along the axis of elongation (Fig 1G). This was evident by comparing the axis of cell division and the principal axis of the region. The angle difference between these axes was smaller in elongating areas compared with non-elongating areas within the same aggregate (Fig 1G). This suggested that polarized cell division accompanied enhanced proliferation during aggregate elongation (Gong et al., 2004; Keller, 2006).

Collagen I becomes reorganized when epithelial aggregates break symmetry

To determine how Collagen 1 drives aggregate elongation, we visualized Collagen 1 by labelling with the collagen-binding peptide CNA35 (mCherry-CNA35; (Krahn et al., 2006)); this was mixed with soluble Collagen I before the incorporation of MCF10A aggregates (Fig 2A). Collagen I, in contrast to the basement membrane-like Matrigel™, is composed of fibrillar polymers that can guide cell movement and whose organization is influenced by the application of cellular forces (Brownfield et al., 2013; Gjorevski et al., 2015; Piotrowski-Daspit et al., 2017). Aggregate

elongation appeared to coincide with change in fibril organization. Whereas fibrils appeared isotropic in acellular gels, collagen condensed around the aggregates that had begun to elongate, forming dense bands that extended away from the cells into the gel.

We then assessed if collagen reorganization correlated with aggregate elongation. First, we measured collagen bundling by using Orientation J to measure the coherency of fibrils, defined as co-orientation in the same direction (see Methods for details). Then we compared coherency of the collagen fibrils with aggregate shape, as measured by the symmetry ratio (Fig 2B). Overall, collagen coherency increased with the symmetry breaking of aggregates, as indicated by an increase in symmetry ratio (Fig 2C). Furthermore, coherency was greater around the elongating protrusions rather than around the rounded areas of the same aggregates (Fig 2D). Aggregates that remained spherical showed no regional differences in collagen organization. Thus, not only did bundles form as aggregates elongated, but the degree of bundling increased with the degree of elongation.

Collagen bundling required cell proliferation, as coherency was reduced by treatment with either Mitomycin C or aphidicolin (Fig 2G,H), implying that proliferation triggered matrix reorganization. Collagen condensation was also reduced when we inhibited cellular contractility with the myosin antagonist, blebbistatin, or the Rho kinase (ROCK) inhibitor, Y27632 (Fig 2I,J). In contrast, Rac1 inhibitor treatment did not affect aggregate elongation and collagen fibril rearrangement (data not shown). This suggested that, as they broke symmetry, aggregates exerted forces to reorganize their local collagen environment.

Collagen polarization orients elongation.

Collagen gels also became increasingly polarized when aggregates elongated. Here we define polarization in terms of the orientation of fibrils relative to a reference axis, which we took as the axis of elongation of the nearby cell aggregate. Using Orientation J, we found that collagen fibrils were more anisotropic around elongating regions of aggregates (Fig 2E). Histograms of fibril orientation showed a broad distribution around non-elongating aggregates, but a peak that corresponded to the aggregate axis at regions of elongation.

To further compare the polarization of the gel and of the cellular aggregates, we extracted the principal axis of collagen orientation, as a measure of collagen polarity, from the distribution histograms of anisotropic gels. Then we compared the principal gel axis with the axis of elongation of the aggregate that it surrounded (Fig 2F). In this analysis, a decrease in the difference in angles between these two axes indicates an increase in their co-alignment. We found that the angle differences between the axes of collagen polarity and aggregate elongation was significantly smaller for elongating than for non-elongating aggregates (Fig 2F). Thus, the collagen matrix became more anisotropic around elongating aggregates, and its polarity appeared to align with the direction in which the aggregate elongated.

We then asked whether polarization in the collagen gel could direct elongation of the aggregate. In other words, whether the polarization of collagen fibrils that

occurred when anlage broke symmetry provided a directional cue for further elongation. For this, we developed a strategy that applied exogenous stretch to polarize the matrix independently of cell-generated forces. In this protocol, a collagen gel was created within a ring-shaped polydimethylsiloxane (PDMS) frame, then stretched uniaxially by expanding a stretcher inserted into the hole of the ring for 4 h (Fig S3A,B). Second harmonic imaging confirmed that collagen fibers were isotropically distributed in the unstretched gels and became bundled (more coherent) and more anisotropic immediately after stretching (Fig S2C, D), with their principal axes oriented in the direction of stretch (Fig S2E). Moreover, polarization of the collagen fibrils could be preserved for at least 7 days after the application of stretch by re-embedding the collagen rings in a larger collagen gel (Fig 3A-C, Fig S3B). In contrast, when gels were allowed to float in medium after stretching (Fig 3D, S3B), gel coherency (Fig 3E) and isotropy (Fig 3F) reverted to that of unstretched gels. This therefore provided an assay to test how polarization of a collagen matrix might influence epithelial elongation.

We then transplanted spherical cell aggregates from Matrigel™ into the collagen rings and applied our stretching protocol. Interestingly, the aggregates did not become elongated during the period when stretch was actively applied. The symmetry ratios of aggregates immediately after stretching were identical to those in unstretched aggregates (Fig S4 A,B). Instead, aggregates broke symmetry many hours after the period of active stretching. However, symmetry breaking occurred earlier when stretched gels were allowed to retain collagen polarization by re-embedding (35.14 ± 3.28 h, Fig 3G,H) compared with aggregates that were allowed to break symmetry spontaneously in non-stretched gels (68.40 ± 5.88 h, $p<0.001$). Aggregate elongation was therefore initiated as a delayed response to external stretch.

Moreover, aggregates elongated preferentially along the axis of the exogenous stretch, whereas aggregates incorporated into non-stretched gels elongated in a random direction (Fig 3G,I, Fig S4D; Movie S2). The angle difference between collagen fiber orientation and aggregate elongation was significantly smaller in gels that had been stretched than in unstretched control gels (Fig 3J). Of note, collagen gel reorganization was preserved (Fig 3K,L), even in the presence of cellular aggregates, and this was oriented in the direction of the original stretch. This suggested that in this assay the elongating aggregates were following the polarity of the gel itself.

Importantly, the impact of stretch on the aggregates was disrupted when collagen polarization was reversed. The proportion of aggregates that elongated after stretching was reduced when the gels were floated rather than being reembedded (Fig 4A) and their length of elongation was reduced (Fig 4B). Of note, cell-based forces could not overcome the external forces acting on the gel as the reversal of collagen polarization occurred even when aggregates were incorporated into the gel (Fig 4C). This implied that collagen polarization may have been responsible for allowing external stretch to promote aggregate elongation.

To confirm that these results were due to a critical role of collagen polarization, rather than as-yet-unknown impacts of stretch upon the cells, we used collagenase to extract aggregates from gels immediately after their 4 h stretch, then transplanted them into unstretched gels where the collagen fibers oriented randomly (Fig 4D). We reasoned that if elongation were due to a cell-intrinsic mechanism that bore the memory of the stretch, then this should be preserved even after cells were transplanted into a naïve gel. As noted earlier, aggregate elongation occurred earlier when stretched gels were reembedded. However, this effect was lost when cells were removed from the stretched gel immediately after stretching and transplanted into a naïve isotropic gel (Fig 4E). Together, these results indicate that collagen polarization can direct aggregate elongation, to accelerate its initiation and orient the direction of symmetry-breaking.

Collagen matrix polarization stimulates cell proliferation for anlagen elongation.

Since cell proliferation was necessary for aggregate elongation, we then asked if collagen polarization by stretch regulated proliferation. Ki-67 positivity was increased in aggregates in gels that had been stretched and then re-embedded to preserve collagen polarization, compared to unstretched gels (Fig 5A). Cell proliferation mediated the enhanced elongation in the stretched gels, as both the length (Fig 5B) and symmetry ratio (Fig 5C) of stretch-stimulated aggregates were reduced by mitomycin C and aphidicolin.

However, proliferation was not increased if gels were allowed to float, rather than being re-embedded, after stretching. Floating the gels reduced the proportion of proliferating cells in the aggregates overall (Fig 5D,E) as well as those specifically within the area of elongation (Fig 5F), compared with gels that had been re-embedded to preserve collagen polarization. This implied that it was polarization of the gel, rather than simply transfer into collagen, that could stimulate cell proliferation to elongate aggregates.

Polarized collagen promotes cell proliferation through the integrin-ERK pathway

Integrins are the major ECM receptors in the mammary gland and other epithelia, which control diverse aspects of cellular function, including cell proliferation (Miranti and Brugge, 2002; Wozniak et al., 2003)(Fig 6B). We therefore asked if integrin signaling stimulated cell proliferation in response to collagen polarization.

We focused on the β1-integrins which have been implicated in regulating cell proliferation during mammary gland development (Li et al., 2005) and include a number of collagen 1 receptors. Indeed, α2β1-integrin, a high-affinity Type 1 collagen receptor (Heino, 2000; Käpylä et al., 2000) was evident in MCF10A cells by Western analysis (Fig 6A). Then we used the inhibitory AIIB2 antibody to block β1-integrin during gel-stretching experiments. mAb AIIB2 (15 μg/ml) was added as aggregates were transplanted into the collagen gel rings and replenished after 7 days. mAb AIIB2 blocked the induction of proliferation and elongation in stretch-

polarized gels (Fig 6C). After 3 days incubation, 49.19 ± 1.61 % aggregates started to elongate in controls, whereas less than 20 % of aggregates elongated when integrin β1 was inhibited (AIIB2: 17.86 ± 4.78 %) (Fig 6C). Aggregates eventually elongated with prolonged culture (comparing the proportion of elongated cells at 7 days compared with 3 days). Even so, those that elongated remained shorter (Fig 6E) and less asymmetric (Fig 6F) than in the absence of AIIB2. This implicated a β1-integrin in mediating a proliferative signal required to drive aggregate elongation from polarized collagen.

Extracellular signal-regulated kinase (ERK) is one of the major pathways that stimulates cell proliferation downstream of integrin adhesion (Fig 6B) (Moreno-Layseca and Streuli, 2014; Streuli and Akhtar, 2009; Walker and Assoian, 2005). We therefore used the inhibitor the ERK inhibitor, FR180204 (50 μM) to test a role for ERK1/2 signalling in MCF10A aggregate elongation. As seen with integrin inhibition, blocking ERK reduced the proportion of aggregates that elongated in response to stretch-induced collagen polarization (Fig 6C,G). As well, the length (Fig 6H) and asymmetry (Fig 6I) were reduced in those that did elongate. These data suggested that polarized collagen stimulated cell proliferation for epithelial elongation via an integrin β1-ERK signaling pathway. In contrast, although Hippo pathway signaling has been implicated in breaking the symmetry of epithelial organoids (Serra et al., 2019) , we did not detect any changes in nuclear Yap1 staining to suggest a role for this pathway in our experiments (Fig S5).

Discussion

Our experiments reveal an interplay between collagen polarization and cell proliferation that can guide epithelial elongation (Fig 7). We found that exposure to a 3D collagen matrix was sufficient to cause non-polarized mammary aggregates to break symmetry and elongate. The initial step of symmetry-breaking was associated with reorganization of collagen fibrils around the aggregate. Fibrils then became increasingly bundled and aligned with the axis of broken symmetry as elongation proceeded. We propose that in this later phase the polarized collagen networks effectively provide a structural memory of the initial axis of symmetry breaking, i.e., a relatively long-lived spatial cue that directs further elongation of the MCF10A anlagen.

The capacity for collagen polarization to direct the elongation of mammary epithelial anlage was confirmed by its role in mediating the impact of external stretch on aggregates. The application of stretching forces accelerated the onset of symmetry breaking and oriented the direction of elongation. But this required that the collagen network be polarized, as the stimulatory effects of stretch were lost when collagen polarization was allowed to revert by floating the gels, or when aggregates were immediately transplanted into a naïve, non-polarized gel. Together, these lead us to conclude that polarization of the collagen matrix directed aggregate elongation in these experiments. Collagen polarization likely relies upon the fibrillar nature of

collagen I, which may further explain why collagen I was better able to stimulate elongation than Matrigel™.

Epithelial tubulogenesis has been proposed to involve the coordinated action of multiple cellular processes. Interestingly, cell proliferation was critical in our experiments. Proliferation was selectively increased in regions of aggregates that were elongating and inhibiting cell division blocked elongation. Moreover, proliferation was necessary for external stretching to stimulate aggregate elongation. While it is likely that processes such as cell migration also contribute, especially in the complex environment *in vivo*, they were not sufficient to compensate for blocking cell division in our experiments.

How, then, does collagen polarization promote cell proliferation? Here, our data point to a key role for integrin-based mitogenic signaling, as collagen polarization failed to induce aggregate elongation or stimulate proliferation when we blocked the β1 integrins or ERK signaling. However, since greater proliferation occurred in stretched gels than in non-stretched gels, this further implied that the cells were responding to a feature of the gels beyond their collagen chemical composition. Indeed, the polarization of collagen networks has complex effects at the cellular scale. Increasing fibril alignment in acellular collagen gels was reported to increase fibre stiffness and decrease pore size (Riching et al., 2014; Taufalele et al., 2019), even in the absence of externally applied forces. Moreover, in single cell cultures aligned collagen fibres were associated with larger focal adhesions than non-aligned fibrils (Doyle and Yamada, 2016). One possibility, then, is that integrin signaling was responding to the increased stiffness of the polarized collagen gels. This is consistent with the well-characterized role for integrins to mediate mechanosensation that responds to in matrix stiffness (Giannone and Sheetz, 2006). As well, collagen 1 can bind to, and sequester, a variety of growth factors. Whether this reservoir can be released when cells apply tension to collagen is an interesting question for consideration (Wipff and Hinz, 2008).

Interestingly, the enhanced proliferation induced by collagen polarization was seen within subregions of aggregates. This regional patterning would be necessary if proliferation drives elongation, as a global increase in cell number would cause aggregates to expand isotropically. One possible explanation for this regional distribution is that the polarized bundling of collagen effectively micropatterns the matrix around the aggregates to orient cell division. Micropatterning experiments using 2-dimensional substrata have shown that anisotropic confinement can orient patterns of cell division (Thery et al., 2005), potentially by orienting tensile stresses, as would also be predicted to accompany stiffer, condensed collagen bundles. Tensile forces have been reported to orient cell division (Campinho et al., 2013; Legoff et al., 2013) and we observed that cell divisions in elongating regions of an aggregate were preferentially aligned with the principal axis of the aggregate to a greater degree than seen in non-elongating areas.

In summary, we suggest that the polarization of a collagen 1 matrix may contribute to elongation of epithelial anlage during tubulogenesis (Fig 7). This could synergize with other guidance factors, such as chemokines and motokines, by

providing long-lasting structural cues that promote regional cell proliferation to guide the direction in which aggregates elongate. While we applied external stretch to experimentally induce collagen polarization, in the native tissue collagen will be reorganized by active processes, including those generated by the epithelial cells themselves. In particular, cell-based forces exerted through integrins can apply strain on collagen fibrils (Hall et al., 2016) and, indeed, we observed that collagen failed to reorganize spontaneously around aggregates when we blocked cell contractility. Thus, collagen polarization may provide a memory of the early anisotropies in the forces that epithelial cells exert upon their surrounding ECM. Whether these anisotropies are stochastic or set by active processes, such as proliferation or migration, will be interesting questions for future research.

Acknowledgements

The authors were supported by the National Health and Medical Research Council of Australia (Fellowship 1136592 and GNT1123816, 1140090 to ASY), Australian Research Council (DP19010287, 190102230 to AY and FT190100516 to SS), a Snow Medical Fellowship to JH, and a postdoctoral fellowship from The Uehara Memorial Foundation to HK.

Materials and Methods

Cell culture and lentivirus infection

MCF10A human mammary epithelial cells were cultured in DMEM/F12 medium supplemented with 5% horse serum, 10 µg/ml insulin, 0.5 µg/ml hydrocortisone, 100 ng/ml cholera toxin, 20 ng/ml EGF, 100 units/ml Penicillin and 100 units/ml Streptomycin as previously described (Debnath et al., 2002).

HEK-293T cells were transfected using Lipofectamine 2000 (Invitrogen) for lentiviral expression vector pLL5.0 and third generation packaging constructs pMDLg/pRRE, RSV-Rev and pMD.G. Third generation packaging constructs were kindly provided by Prof. James Bear (UNC Chapel Hill, North Carolina, USA). After transducing MCF10A cells with either pLL5.0-EGFP-HRasC20 or pLL5.0-NLS-mCherry lentivirus construct, we isolated highly-expressing cells using Fluorescence-activated cell sorting (Influx Cell sorter; Cytopeia).

3D Matrigel and collagen culture

MCF10A aggregates and acini were cultured on 100% growth factor reduced Matrigel (FAL354230; Corning) and overlayed with Matrigel including medium in 8 well chamber coverglass (0030742036; Eppendorf) as previously described (Debnath et al., 2002; Debnath et al., 2003). In brief, single isolated MCF10A cells were mixed with an assay medium containing 2% Matrigel, 5 ng/ml EGF and seeded on a solidified layer of 100% Matrigel at 10000 cells/well. After seeding cells on Matrigel, medium was changed every 4 days.

In collagen culture, single isolated MCF10A cells were mixed with collagen gel at 20000 cells/well (FAL354236; Corning). This mixture was neutralized with NaOH and HEPES buffer and collagen concentration was adjusted to 1.0 mg/ml with culture

medium on ice. The pH of collagen solution was checked by litmus paper. Collagen solution with cells was seeded in 8 well chamber coverglass and solidified at 37 □ for 30 min.

Transplantation of MCF10A aggregates

MCF10A aggregates cultured on Matrigel for 10 days were washed with PBS and incubated with cold cell recovery solution (FAL354253; Corning) for 30 min on ice. Aggregates were collected into a tube containing the cell recovery solution, spun down at 1200 rpm, and washed with cold PBS. PBS-washed aggregates were resuspended in MCF10A culture medium and mixed with collagen solution neutralized with NaOH and HEPES buffer. Collagen gel solution with aggregates were solidified at 37 □ for 30 min.

Aggregates embedded in collagen gel were isolated from gel by dissolving the gel with collagenase (C2799; Sigma). Gels were washed with PBS and incubated in 20 µg/ml collagenase in Hanks' Balanced Salt Solution (H8264; Sigma) at 37 □ for 30 min to dissolve the collagen gel. Aggregates were collected with incubated solution into the tube and mixed with DMEM/F12 medium which contains 20% horse serum. Solution was spun down at 1200 rpm and pellet was washed with PBS. PBS-washed aggregates were resuspended in culture medium and re-embedded in collagen gel.

Plasmids

pLL5.0-NLS-mCherry was constructed in previous study (Leerberg et al., 2014). pLL5.0-EGFP-HRasC20 was generated by insertion of EGFP-HRasC20 fragment which was amplified from pEGFP-F (#6074-1; Clontech) by PCR into pLL5.0 vector. pLL5.0-EGFP (gift from Prof. James Bear; UNC Chapel Hill, North Carolina, USA) was digested with EcoRI and SbfI to remove EGFP, and then EGFP-C20 fragment was inserted and ligated by In-Fusion cloning kit (638910; Clontech).

Antibodies and inhibitors

Primary antibodies used for immunocytochemistry in this study were rabbit anti-Ki67 (ab15580; Abcam), mouse anti-laminin V (MAB19562; Chemicon), rat anti-E-cadherin (131900; Invitrogen), and mouse anti-GM130 (610822; BD) and rabbit anti-YAP1 (4912; Cell Signaling Technology). F-actin was stained with AlexaFluor 488-, 594-, 647-phalloidin (Invitrogen). Primary antibodies used for immunoblot were rabbit anti-integrin α2 (ab181548; Abcam), mouse anti-integrin β1 (610467; BD Transduction Laboratories) and rabbit anti-p44/42 MAPK (Erk1/2) (9102; Cell Signaling Technology). AIIB2 antibody for blocking integrin β 1 was purchased from Developmental Studies Hybridoma Bank and treated at 15 µg/ml in this study.

Proliferation inhibitors mitomycin C (M7949; Sigma) and aphidicolin (178273; Merck) were used at 10 µM and 2 µM respectively. Myosin II inhibitor blebbistatin (203390; Sigma) and ROCK inhibitor Y-27632 (688000; Sigma) were used at 25 µM and 30 µM respectively. ERK1/2 inhibitor FR180204 (SC-203945; Santa Cruz) was used at 50 µM. Except for mitomycin C, cell aggregates were treated with the inhibitors after transplantation into collagen gels. Inhibitors were then replenished when medium was changed and left in the collagen culture until cell aggregates were ready to be fixed. For mitomycin C wash out experiments, cell aggregates were treated with mitomycin C for 1 hour, then washed 3 times with PBS and left to recover in MCF10A culture medium.

Immunocytochemistry and microscopy

3D cultured cells in gel were fixed with 4% paraformaldehyde in cytoskeleton stabilization buffer (10mM PIPES at pH 6.8, 100mM KCl, 300 mM sucrose, 2 mM EGTA and 2 mM $MgCl_2$) at room temperature for 30 min, followed by a treatment for 30 min with 0.5% TritonX-100 and 10% goat serum in PBS for 1 hour at room temperature. Then they were stained with primary antibodies for overnight at 4 □. Subsequently, cells were washed with PBS and incubated with secondary antibodies with phalloidin and DAPI for 1 hour at room temperature.

Confocal images were acquired with an upright Meta laser scanning confocal microscope (LSM710; Zeiss) equipped with plan-Apochromat 20x 0.8NA or 40x 1.3NA objectives (Zeiss) and zen2012 software (Zeiss). The fluorescent images of collagen fibrils probed with mCherry-CNA35 were acquired by inverted microscope (Ti2; Nikon) equipped with Dragonfly spinning disc (Andor), by using plan-Apo 10x 0.45NA, 20x 0.75NA or 40x 0.95NA dry objectives (Nikon) and Fusion software (Andor).

Fluorescent Images of the SHG signal from collagen-1 were collected with an inverted confocal microscope (LSM710; Zeiss) equipped with multiphoton laser by using 860 nm excitation with SHG signal obtained with 690 nm bandpass filter. A 40x 1.3NA or 63x 1.40NA plan-apochromat oil objectives (Zeiss) were used to obtain SHG signals.

Fluorescence and phase contrast live images of elongating aggregates were acquired with an inverted fluorescence microscope (IX81; Olympus) equipped with CCD-camera (Hamamatsu) and an incubation box (Clear State Solutions) maintained at 37□ and 5% CO_2 with gas controller (OkoLab), using plan-Apo 10x 0.4NA objective (Olympus) and CellSens software (Olympus).

Collagen gel labeling and stretching

Collagen fibrils were labelled with mCherry-CNA35 by mixing with purified mCherry-CNA35 protein at 2 μM before gelling. Gels were solidified at 37 □ for 30 min.

PDMS gel frame and stretchers for gel stretching were kindly gifted from Dr. James Hudson (QIMR Berghofer, Queensland, Australia). 1.5 mg/ml collagen gels were solidified as a ring-shape in PDMS frame. PDMS stretchers were inserted into the hole of the gel and expanded, and incubated for 4 hours in culture medium. Stretched gels were released and then floated in medium or re-embedded in collagen gel. For re-embedding, stretched gels were put in 1.5 mg/ml collagen gel and solidified at at 37 □ for 30 min.

CNA35-mcherry protein purification

Protein expression vector pET28a-mCherry-CNA35 was obtained from Addgene (#61607). Transformed E.coli (BL21) was cultured in 400 ml LB, and induced protein expression with isopropyl β-D-1-tthiogalactopyranoside for 20 hours at 25□. Cultured bacteria were spun down, and collected bacteria pellet was sonicated. The lysate was centrifuged and the resulting supernatant was run through a column filled with N-NTA His-band resin (Millipore). Bound protein was eluted and then dialyzed for overnight in PBS at 4□. Endotoxin was removed by endotoxin removal columns (88274; Thermo) following with manufacturer's protocol.

Quantitative analysis of collagen fibril alignment and aggregates elongation

Fluorescent confocal images of collagen fibrils acquired SHG microscopy or CNA35 probes were used for collagen fibril analysis. We used Orientation J to characterize three features in the organization of collagen fibrils orientations (Clemons et al.,

2018): i) The coherency of fibrils, defined as co-orientation in the same direction, as a measure of bundling. ii) Isotropy, the distribution of fibril orientation in the field of analysis; and iii) Polarization, defined as the principal axis of fibril orientation in anisotropic gels, relative to a reference axis. 50 X 50 um or 100 X 100 um size of ROI were selected from SHG images or CNA35 probed images respectively and used for analysis. Elongation axis of aggregates were measured by the angle tool in ImageJ, and then we calculated the angle difference between principal axis of collagen fibrils or stretching axis.

The symmetry ratio of aggregates was measured by dividing the longest length by widest width of aggregates.

Quantitative analysis of proliferating cells and nuclear division angle

The number of cells co-stained with DAPI and anti-Ki67 antibody were counted by Imaris software (Bitplane). The number of Ki67 positive cells were divided by the total number of nucleus stained with DAPI to calculate percentage of Ki67 positive cells. For live imaging, cells expressed with NLS-mCherry to count their number. The frequency and orientation of cell division were analyzed from the time lapse images by ImageJ. We set the elongation axis of aggregate as a reference and measured the angle difference between elongation axis and dividing axis of nucleus.

Analysis of cellular motility

To obtain the migration speed of cells, we tracked individual cell nuclei using the Spot function in the Imaris software (Huebner et al., 2016). The fluorescent images of cells expressing NLS-mCherry were acquired every 10 minutes for at least 50 hours.

Statistical analysis

Significance was determined by unpaired Student's t test and one-way ANOVA by using GraphPad Prism 8 (GraphPad software).

References

Affolter, M., Zeller, R., and Caussinus, E. (2009). Tissue remodelling through branching morphogenesis. Nat Rev Mol Cell Biol *10*, 831-842.

Andrew, D.J., and Ewald, A.J. (2010). Morphogenesis of epithelial tubes: Insights into tube formation, elongation, and elaboration. Dev Biol *341*, 34-55.

Bastidas-Ponce, A., Scheibner, K., Lickert, H., and Bakhti, M. (2017). Cellular and molecular mechanisms coordinating pancreas development. Development *144*, 2873-2888.

Brownfield, D.G., Venugopalan, G., Lo, A., Mori, H., Tanner, K., Fletcher, D.A., and Bissell, M.J. (2013). Patterned collagen fibers orient branching mammary epithelium through distinct signaling modules. Curr Biol *23*, 703-709.

Buchmann, B., Meixner, L.K., Fernandez, P., Hutterer, F.P., Raich, M.K., Scheel, C.H., and Bausch, A.R. (2019). Mechanical plasticity of the ECM directs invasive branching morphogenesis in human mammary gland organoids. bioRxiv, 860015.

Campinho, P., Behrndt, M., Ranft, J., Risler, T., Minc, N., and Heisenberg, C.P. (2013). Tension-oriented cell divisions limit anisotropic tissue tension in epithelial spreading during zebrafish epiboly. Nat Cell Biol *15*, 1405-1414.

590 Chung, S., and Andrew, D.J. (2008). The formation of epithelial tubes. Journal of Cell Science
591 *121*, 3501-3504.
592 Clemons, T.D., Bradshaw, M., Toshniwal, P., Chaudhari, N., Stevenson, A.W., Lynch, J., Fear,
593 M.W., Wood, F.M., and Iyer, K.S. (2018). Coherency image analysis to quantify collagen
594 architecture: implications in scar assessment. Rsc Adv *8*, 9661-9669.
595 Costantini, F., and Kopan, R. (2010). Patterning a complex organ: branching morphogenesis
596 and nephron segmentation in kidney development. Dev Cell *18*, 698-712.
597 Debnath, J., Mills, K.R., Collins, N.L., Reginato, M.J., Muthuswamy, S.K., and Brugge, J.S.
598 (2002). The role of apoptosis in creating and maintaining luminal space within normal and
599 oncogene-expressing mammary acini. Cell *111*, 29-40.
600 Debnath, J., Muthuswamy, S.K., and Brugge, J.S. (2003). Morphogenesis and oncogenesis of
601 MCF-10A mammary epithelial acini grown in three-dimensional basement membrane
602 cultures. Methods *30*, 256-268.
603 Doyle, A.D., and Yamada, K.M. (2016). Mechanosensing via cell-matrix adhesions in 3D
604 microenvironments. Exp Cell Res *343*, 60-66.
605 Economou, A.D., Brock, L.J., Cobourne, M.T., and Green, J.B. (2013). Whole population cell
606 analysis of a landmark-rich mammalian epithelium reveals multiple elongation mechanisms.
607 Development *140*, 4740-4750.
608 Frantz, C., Stewart, K.M., and Weaver, V.M. (2010). The extracellular matrix at a glance. J
609 Cell Sci *123*, 4195-4200.
610 Giannone, G., and Sheetz, M.P. (2006). Substrate rigidity and force define form through
611 tyrosine phosphatase and kinase pathways. Trends in Cell Biology *16*, 213-223.
612 Gjorevski, N., and Nelson, C.M. (2010). Branch formation during organ development. Wiley
613 Interdiscip Rev Syst Biol Med *2*, 734-741.
614 Gjorevski, N., Piotrowski, A.S., Varner, V.D., and Nelson, C.M. (2015). Dynamic tensile forces
615 drive collective cell migration through three-dimensional extracellular matrices. Sci Rep *5*,
616 11458.
617 Gong, Y., Mo, C., and Fraser, S.E. (2004). Planar cell polarity signalling controls cell division
618 orientation during zebrafish gastrulation. Nature *430*, 689-693.
619 Graham, M.F., Diegelmann, R.F., Elson, C.O., Lindblad, W.J., Gotschalk, N., Gay, S., and Gay,
620 R. (1988). Collagen content and types in the intestinal strictures of Crohn's disease.
621 Gastroenterology *94*, 257-265.
622 Guo, C.L., Ouyang, M., Yu, J.Y., Maslov, J., Price, A., and Shen, C.Y. (2012). Long-range
623 mechanical force enables self-assembly of epithelial tubular patterns. Proc Natl Acad Sci U S
624 A *109*, 5576-5582.
625 Hall, M.S., Alisafaei, F., Ban, E., Feng, X., Hui, C.-Y., Shenoy, V.B., and Wu, M. (2016). Fibrous
626 nonlinear elasticity enables positive mechanical feedback between cells and ECMs.
627 Proceedings of the National Academy of Sciences *113*, 14043-14048.
628 Harunaga, J., Hsu, J.C., and Yamada, K.M. (2011). Dynamics of salivary gland morphogenesis.
629 J Dent Res *90*, 1070-1077.
630 Heino, J. (2000). The collagen receptor integrins have distinct ligand recognition and
631 signaling functions. Matrix Biology *19*, 319-323.
632 Huebner, R.J., Neumann, N.M., and Ewald, A.J. (2016). Mammary epithelial tubes elongate
633 through MAPK-dependent coordination of cell migration. Development *143*, 983-993.
634 Ingman, W.V., Wyckoff, J., Gouon-Evans, V., Condeelis, J., and Pollard, J.W. (2006).
635 Macrophages promote collagen fibrillogenesis around terminal end buds of the developing
636 mammary gland. Dev Dyn *235*, 3222-3229.

637 Iruela-Arispe, M.L., and Beitel, G.J. (2013). Tubulogenesis. Development *140*, 2851-2855.
638 Kanematsu, A., Marui, A., Yamamoto, S., Ozeki, M., Hirano, Y., Yamamoto, M., Ogawa, O.,
639 Komeda, M., and Tabata, Y. (2004). Type I collagen can function as a reservoir of basic
640 fibroblast growth factor. Journal of Controlled Release *99*, 281-292.
641 Käpylä, J., Ivaska, J., Riikonen, R., Nykvist, P., Pentikäinen, O., Johnson, M., and Heino, J.
642 (2000). Integrin alpha(2)I domain recognizes type I and type IV collagens by different
643 mechanisms. J Biol Chem *275*, 3348-3354.
644 Keely, P.J., Wu, J.E., and Santoro, S.A. (1995). The spatial and temporal expression of the
645 alpha 2 beta 1 integrin and its ligands, collagen I, collagen IV, and laminin, suggest important
646 roles in mouse mammary morphogenesis. Differentiation *59*, 1-13.
647 Keller, R. (2002). Shaping the vertebrate body plan by polarized embryonic cell movements.
648 Science *298*, 1950-1954.
649 Keller, R. (2006). Mechanisms of elongation in embryogenesis. Development *133*, 2291-
650 2302.
651 Krahn, K.N., Bouten, C.V., van Tuijl, S., van Zandvoort, M.A., and Merkx, M. (2006).
652 Fluorescently labeled collagen binding proteins allow specific visualization of collagen in
653 tissues and live cell culture. Anal Biochem *350*, 177-185.
654 Krause, S., Maffini, M.V., Soto, A.M., and Sonnenschein, C. (2008). A novel 3D in vitro culture
655 model to study stromal-epithelial interactions in the mammary gland. Tissue Eng Part C
656 Methods *14*, 261-271.
657 Leerberg, J.M., Gomez, G.A., Verma, S., Moussa, E.J., Wu, S.K., Priya, R., Hoffman, B.D.,
658 Grashoff, C., Schwartz, M.A., and Yap, A.S. (2014). Tension-sensitive actin assembly supports
659 contractility at the epithelial zonula adherens. Curr Biol *24*, 1689-1699.
660 Legoff, L., Rouault, H., and Lecuit, T. (2013). A global pattern of mechanical stress polarizes
661 cell divisions and cell shape in the growing Drosophila wing disc. Development *140*, 4051-
662 4059.
663 Li, N., Zhang, Y., Naylor, M.J., Schatzmann, F., Maurer, F., Wintermantel, T., Schuetz, G.,
664 Mueller, U., Streuli, C.H., and Hynes, N.E. (2005). β1 integrins regulate mammary gland
665 proliferation and maintain the integrity of mammary alveoli. The EMBO Journal *24*, 1942-
666 1953.
667 Llacua, L.A., Faas, M.M., and de Vos, P. (2018). Extracellular matrix molecules and their
668 potential contribution to the function of transplanted pancreatic islets. Diabetologia *61*,
669 1261-1272.
670 Miranti, C.K., and Brugge, J.S. (2002). Sensing the environment: a historical perspective on
671 integrin signal transduction. Nature Cell Biology *4*, E83-E90.
672 Moreno-Layseca, P., and Streuli, C.H. (2014). Signalling pathways linking integrins with cell
673 cycle progression. Matrix Biology *34*, 144-153.
674 Nakanishi, Y., Sugiura, F., Kishi, J., and Hayakawa, T. (1986). Collagenase inhibitor stimulates
675 cleft formation during early morphogenesis of mouse salivary gland. Dev Biol *113*, 201-206.
676 Nerger, B.A., and Nelson, C.M. (2018). 3D culture models for studying branching
677 morphogenesis in the mammary gland and mammalian lung. Biomaterials.
678 Patel, V.N., Rebustini, I.T., and Hoffman, M.P. (2006). Salivary gland branching
679 morphogenesis. Differentiation *74*, 349-364.
680 Piotrowski-Daspit, A.S., Nerger, B.A., Wolf, A.E., Sundaresan, S., and Nelson, C.M. (2017).
681 Dynamics of Tissue-Induced Alignment of Fibrous Extracellular Matrix. Biophys J *113*, 702-
682 713.

683 Price, R.G., and Spiro, R.G. (1977). Studies on the metabolism of the renal glomerular
684 basement membrane. Turnover measurements in the rat with the use of radiolabeled
685 amino acids. J Biol Chem *252*, 8597-8602.
686 Riching, K.M., Cox, B.L., Salick, M.R., Pehlke, C., Riching, A.S., Ponik, S.M., Bass, B.R., Crone,
687 W.C., Jiang, Y., Weaver, A.M., *et al.* (2014). 3D collagen alignment limits protrusions to
688 enhance breast cancer cell persistence. Biophys J *107*, 2546-2558.
689 Schedin, P., and Keely, P.J. (2011). Mammary gland ECM remodeling, stiffness, and
690 mechanosignaling in normal development and tumor progression. Cold Spring Harb
691 Perspect Biol *3*, a003228.
692 Schottenfeld, J., Song, Y., and Ghabrial, A.S. (2010). Tube continued: morphogenesis of the
693 Drosophila tracheal system. Curr Opin Cell Biol *22*, 633-639.
694 Serra, D., Mayr, U., Boni, A., Lukonin, I., Rempfler, M., Challet Meylan, L., Stadler, M.B.,
695 Strnad, P., Papasaikas, P., Vischi, D., *et al.* (2019). Self-organization and symmetry breaking
696 in intestinal organoid development. Nature *569*, 66-72.
697 Shi, M., Zhu, J., Wang, R., Chen, X., Mi, L., Walz, T., and Springer, T.A. (2011). Latent TGF-
698 beta structure and activation. Nature *474*, 343-349.
699 Shi, Q., Ghosh, R.P., Engelke, H., Rycroft, C.H., Cassereau, L., Sethian, J.A., Weaver, V.M., and
700 Liphardt, J.T. (2014). Rapid disorganization of mechanically interacting systems of mammary
701 acini. Proc Natl Acad Sci U S A *111*, 658-663.
702 Simon-Assmann, P., Kedinger, M., De Arcangelis, A., Rousseau, V., and Simo, P. (1995).
703 Extracellular matrix components in intestinal development. Experientia *51*, 883-900.
704 Soliman, N.A., and Yussif, S.M. (2016). Ki-67 as a prognostic marker according to breast
705 cancer molecular subtype. Cancer Biol Med *13*, 496-504.
706 Sternlicht, M.D., Kouros-Mehr, H., Lu, P., and Werb, Z. (2006). Hormonal and local control of
707 mammary branching morphogenesis. Differentiation *74*, 365-381.
708 Streuli, Charles H., and Akhtar, N. (2009). Signal co-operation between integrins and other
709 receptor systems. Biochemical Journal *418*, 491-506.
710 Taufalele, P.V., VanderBurgh, J.A., Munoz, A., Zanotelli, M.R., and Reinhart-King, C.A. (2019).
711 Fiber alignment drives changes in architectural and mechanical features in collagen matrices.
712 PLoS One *14*, e0216537.
713 Thery, M., Racine, V., Pepin, A., Piel, M., Chen, Y., Sibarita, J.B., and Bornens, M. (2005). The
714 extracellular matrix guides the orientation of the cell division axis. Nat Cell Biol *7*, 947-953.
715 Tucker, A.S. (2007). Salivary gland development. Semin Cell Dev Biol *18*, 237-244.
716 Varner, V.D., and Nelson, C.M. (2014). Cellular and physical mechanisms of branching
717 morphogenesis. Development *141*, 2750-2759.
718 Verzijl, N., DeGroot, J., Thorpe, S.R., Bank, R.A., Shaw, J.N., Lyons, T.J., Bijlsma, J.W., Lafeber,
719 F.P., Baynes, J.W., and TeKoppele, J.M. (2000). Effect of collagen turnover on the
720 accumulation of advanced glycation end products. J Biol Chem *275*, 39027-39031.
721 Walker, J.L., and Assoian, R.K. (2005). Integrin-dependent signal transduction regulating
722 cyclin D1 expression and G1 phase cell cycle progression. Cancer and Metastasis Reviews *24*,
723 383-393.
724 Wipff, P.J., and Hinz, B. (2008). Integrins and the activation of latent transforming growth
725 factor beta1 - an intimate relationship. Eur J Cell Biol *87*, 601-615.
726 Wozniak , M.A., Desai , R., Solski , P.A., Der , C.J., and Keely , P.J. (2003). ROCK-generated
727 contractility regulates breast epithelial cell differentiation in response to the physical
728 properties of a three-dimensional collagen matrix. Journal of Cell Biology *163*, 583-595.
729

Figure legends

Figure 1. Type 1 collagen induces elongation of MCF10A anlage via cell proliferation.

(A) Cartoon of transplant experiment of MCF10A cell aggregates from Matrigel™ into collagen gel. Single isolated cells are cultured on Matrigel™ and overlayed with Matrigel™-containing medium. Matrigel™ is washed out after 10 days and re-embedded into type-1 collagen gel.

(B) Time lapse images of MCF10A aggregates after transferred into collagen gel. Red arrowheads: elongation from aggregates.

(C) Fluorescence image of elongated aggregate cultured for 8 days after transfer into collagen gel. Aggregate is co-stained with anti-Ki67 antibody (green), phalloidin (magenta) and DAPI (blue). Blue parenthesis: non-elongating area, red parenthesis: elongating area. Scale bar: 100 µm.

(D) Percentage of number Ki67 positive cells in elongating area and non-elongating area of the elongated aggregates. (n = 15 aggregates).

(E) Time lapse images of elongating aggregates expressed with NLS-mCherry. Yellow arrowheads: dividing nucleus. Scale bar: 100 µm.

(F) Frequency of cell division. (n = 12 aggregates).

(G) Average angle of cell division. Elongating axis is 0°. (n = 12 aggregates).

(H) Fluorescent images of MCF10A aggregates co-stained with anti-Ki67 antibody (green) and DAPI (blue). Aggregates are cultured for 0 day (i) or 8 days (ii-iv) after treatment with vehicle (ii), mitomycin C (iii) or aphidicolin (iv). Scale bars: 50 µm in (i, iii, iv), 100 µm in (ii).

(I) Percentage of Ki67 positive cells in aggregates cultured for 1 day or 8 days with or without the treatment of mitomycin C and aphidicolin. (n = 63 aggregates).

(J) Symmetry ratio of aggregates cultured for 1 day or 8 days with or without the treatment of mitomycin C and aphidicolin. (n = 237 aggregates).

Data in (D, F, G, I, J) represent means ± SEM, *P<0.05, **P<0.01, ***P<0.001.

Figure 2. Mammary cell aggregates polarize the ECM during their elongation.

(A) Fluorescent image of collagen fiber alignment and elongated aggregate expressing GFP-HRasC20 which localizes cellular membrane. Collagen fibers are labeled with mCherry-CNA35 peptide. Scale bar: 200 µm.

(B) Cartoon of symmetry ratio of aggregates (i) and gel coherency (ii).

(C) Scatter plot of aggregates symmetry ration and collagen fiber coherency. (n = 75 aggregates).

(D) Coherency of collagen fiber in non-elongating ECM area (blue square) and elongating ECM area (red square) surrounding with elongated aggregates (n = 57 aggregates) or rounded aggregates (n = 19 aggregates).

(E) Distribution of collagen fiber orientation surrounding with elongated aggregates (n = 22 aggregates) or non-elongated aggregates (n = 13 aggregates).
(F) Difference between elongating axis of aggregates and average angle of collagen fibers in non-elongating area or elongating area. (n = 57 aggregates).
(G) Fluorescent images of collagen fibers labeled with mCherry-CNA35 and aggregates expressing GFP-HRasC20 cultured for 8 days with mitomycin C or aphidicolin. Scale bars: 100 μm.
(H) Coherency of collagen fibers surrounding the aggregates treated with mitomycin C and aphidicolin. (n = 40 aggregates).
(I) Fluorescent images of collagen fiber alignment with aggregates expressing GFP-HRasC20 treated with blebbistatin and Y-27632 for 8 days. Scale bars: 200 μm.
(J) Symmetry ratio of aggregates cultured for 8 days with or without the treatment of blebbistatin and Y-27632. (n = 88 aggregates).
Data in (D-F, H, J) represent means ± SEM, **P<0.01, ***P<0.001.

Figure 3. Collagen polarization induces mammary aggregate elongation.
(A) Second harmonic generation (SHG) images of collagen fibers in the gel with or without stretching and incubated for 7 days after re-embedding in gel. Double head arrow: stretching axis. Scale bar: 20um.
(B) Coherency of collagen fiber in the gel with or without stretching. (n = 24 positions in multiple gels).
(C) Distribution of collagen fiber orientation in the gel with or without stretching. (N = 3 independent experiments).
(D) SHG images of collagen fiber floated for 7 days with or without after stretching. Double head arrow: stretching axis. Scale bar: 10 μm.
(E) Coherency of collagen fiber in 7 days floated gel with or without stretching. (n = 46 positions in multiple gels).
(F) Distribution of collagen fiber orientation in 7 days floated gel with or without stretching. (N = 3 independent experiments).
(G) Time lapse images of aggregates embedded in stretched gel. Double head arrow: stretching axis. Scale bar: 200 μm.
(H) Initiation time of aggregates elongation in the gel with or without stretching. (-Stretch: n = 25 aggregates, +Stretch: n = 71 aggregates).
(I) Distribution of elongation axis of aggregates in the gel with or without stretching. (-Stretch: n = 112 aggregates, +Stretch: n = 115 aggregates).
(J) Difference between elongating axis of aggregates and average angle of collagen fibers in the gel with or without stretching. (- Stretch: n = 21 aggregates, +Stretch: n = 102 aggregates).
(K) Fluorescence image of aggregates cultured for 5 days after gel stretching and co-stained with phalloidin and DAPI in stretched gel. Scale bar: 100 μm.
(L) Coherency of collagen fibers surrounding with elongated aggregates in the gel with or without stretching. (- Stretch: n = 21 aggregates, +Stretch: n = 102 aggregates).

Data in (B, C, E, F, H-J, L) represent means ± SEM; ns, not significant, **P<0.01, ***P<0.001.

Figure 4. Collagen polarization must be sustained for mammary aggregate elongation.

(A) Population of elongated aggregates in the re-embedded or floated gel. (N = 3 independent experiments).

(B) The length of elongated aggregates in the re-embedded or floated gel. (N = 3 independent experiments).

(C) Coherency of collagen fibers surrounding the aggregates in the gel re-embedded or floated for 7 days after stretching. (n = 68 aggregates).

(D) Cartoon of aggregates transfer experiment from stretched gel into normal collagen gel. Aggregates are isolated from stretched gel by collagenase and re-embedded in naive gel.

(K) Initiation time of aggregates elongation in the non-stretched gel, stretched gel and normal gel (n = 83 aggregates).

Data in (A-C,E) represent means ± SEM; n.s, not significant, **P<0.01, ***P<0.001.

Figure 5. Collagen polarization induces cell proliferation for aggregate elongation.

(A) Percentage of Ki67 positive cells in aggregates cultured for 8 days in the gel with or without stretching. (n = 49 aggregates)

(B) Length and (C) symmetry ratio of aggregates in stretched gel incubated with mitomycin C or aphidicolin for 8 days. (n = 214)

Data in (B, C, E, G-K) represent means ± SEM; ns, not significant, **P<0.01, ***P<0.001.

(D) Fluorescence images of elongated aggregates cultured for 7 days in the re-embedded or floated gel after stretching. Aggregates are co-stained with anti-Ki67 antibody, Phalloidin and DAPI. Collagen fibers are labeled with mCherry-CNA35.

(E) Percentage of Ki67 positive cells in the aggregates cultured for 7 days in the re-embedded or floated gel after stretching. (n = 56 aggregates).

(F) Percentage of Ki67 positive cells in the elongating area of aggregates in the re-embedded or floated gel. (n = 47 aggregates).

Data in (A-C, E, F) represent means ± SEM; **P<0.01, ***P<0.001.

Figure 6. Collagen polarization promotes cell proliferation through the integrin-ERK pathway.

(A) Immunoblot of integrin α2, β1 and ERK1/2 protein levels in MCF10A cell lysate.

(B) Summary of integrin-ERK pathway to accelerate cell proliferation.

(C) Fluorescent images of aggregates cultured for 7 days treated with AIIB2 antibody or FR180207 after gel stretching. Aggregates are co-stained with anti-Ki67 antibody, Phalloidin and DAPI. Collagen fibers are labeled with mCherry-CNA35. Bars: 100 μm.

(D) Population of elongated aggregates in stretched gel incubated with AIIB2 antibody for 3 days and 7 days. (N = 3 independent experiments).
(E) Length and (F) symmetry ratio of elongated aggregates incubated with AIIB2 antibody for 7 days. (n = 134 aggregates).
(G) Population of elongated aggregates in stretched gel incubated with FR180207 for 3 days and 7 days. (N = 3 independent experiments).
(H) Length and (I) symmetry ratio of elongated aggregates incubated with FR180207 for 7 days. (n = 166 aggregates).
Data in (D-I) represent means ± SEM; ns, not significant, **P<0.01, ***P<0.001.

Figure 7. Model of collagen polarization as a structural memory for epithelial anlage elongation.
(i) Initially isotropic epithelia anlage exert isotropic patterns of force on a non-polarized collagen 1 gel.
(ii) Initial anisotropies in force associated with symmetry-breaking of the aggregate exert strain on collagen fibrils leading to bundling and polarization.
(iii) The polarized collagen matrix provide a structural memory, that promotes regional cell proliferation to direct further elongation of the anlage.

Supplemental Figures

Figure S1. 3D morphology of MCF10A cells.
(A) MCF10A cells cultured in Matrigel^{TM} for 7 days (left) and 31 days (right). Day 7 aggregate is co-stained with anti-E-cadherin antibody (green), anti-GM130 antibody (red), phalloidin (magenta) and DAPI (blue). Day 31 acini is co-stained with anti-Laminin V antibody (green), anti-E-cadherin antibody (red) and DAPI (blue).
(B) MCF10A cells cultured in Type 1 collagen gel for 3 days (left) and 10 days (right). Day 3 MFC10A cells expressing GFP-HRasC20 is co-stained with anti-GM130 antibody (red), phalloidin (magenta) and DAPI (blue). Day 10 MCF10A cells are co-stained with phalloidin (magenta) and DAPI (blue).
(C) MCF10A aggregates transferred from Matrigel^{TM} into collagen gel at day 0 (left) and at day 4 (right). Day 0 aggregate is co-stained with anti-Laminin V antibody (green), anti-E-cadherin antibody (red), and DAPI (blue). Day 4 aggregate is co-stained with anti-Laminin V antibody (green), anti-E-cadherin antibody (red), phalloidin (magenta), and DAPI (blue). *: Y-Z slice image of yellow line.

Figure S2. Cell motility during aggregates elongation.
(A) Nuclear tracking during aggregates elongation. Tails show last 120 min path. Scale bar: 100 µm.
(B) Speed of nuclear motility. (n = 7 movies). Data in (B) represents means ± SEM; ns, not significant.

Figure S3. External gel stretching aligns collagen fiber.
(A) PDMS gel frame and stretching device.

(B) Schematic image of stretching experiment. Gel was stretched for 4 hours and then re-embedded in gel or floated in culture medium for 7 days.
(C) Second harmonic generation microscopy images of collagen gel with or without stretch. Double head arrow: stretching axis.
(D) Coherency of collagen fibers in gel and (E) distribution of fiber orientation. (N = 4 independent experiments)
Data in (D, E) represent means ± SEM; **P<0.01, ***P<0.001.

Figure S4. MCF10A aggregates elongate along the gel stretching axis.
(A) MCF10A aggregates in the gel after 4 hours stretching. Scale bar: 50 μm. Aggregate is co-stained with Phalloidin and DAPI. Collagen fibers are labeled with mCherry-CNA35.
(B) Symmetry ratio of aggregates with or without gel stretching for 4 hours (n = 274 aggregates).
(C) Schematic image of measurement of elongation angle.
(D) The average angle of elongated aggregates in non-stretched gel and stretched gel. (n = 227 aggregates).
Data in (B, D) represent means ± SEM; ns, not significant, ***P<0.001.

Figure S5. YAP1 localization in MCF10A aggregate.
(A) YAP1 localization in rounded MCF10A aggregate cultured for 1 day after transfer into collagen gel. Scale bar: 50 μm.
(B) YAP1 localization in elongated MCF10A aggregate cultured for 8 days after transfer into collagen gel. Scale bar: 100 μm.
Aggregates are co-stained with anti-YAP1 antibody (green), phalloidin (magenta) and DAPI (blue).

Movie S1. Time lapse images of MCF10A aggregates after transferred into collagen gel.
Images were taken every 10 minutes.

Movie S2. Time lapse images of aggregates embedded in stretched gel.
Images were taken every 1 hour.

Fig.1

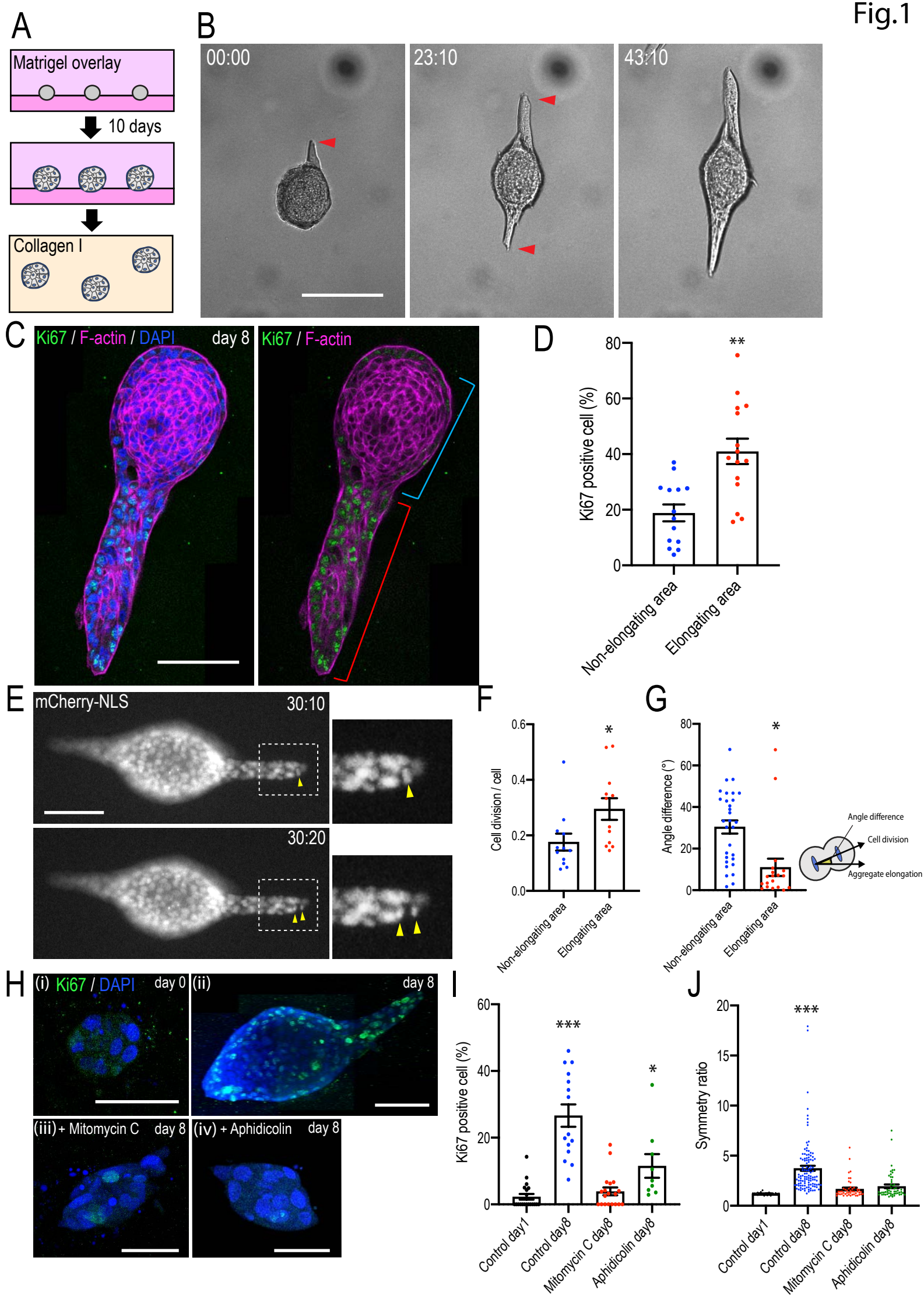
A
Matrigel overlay
10 days
Collagen I
B
00:00
23:10
43:10
C
Ki67 / F-actin / DAPI
day 8
Ki67 / F-actin
D
Ki67 positive cell (%)
Non-elongating area
Elongating area
E
mCherry-NLS
30:10
30:20
F
Cell division / cell
Non-elongating area
Elongating area
G
Angle difference (°)
Angle difference
Cell division
Aggregate elongation
Non-elongating area
Elongating area
H
(i) Ki67 / DAPI
day 0
(ii)
day 8
(iii) + Mitomycin C
day 8
(iv) + Aphidicolin
day 8
I
Ki67 positive cell (%)
Control day1
Control day8
Mitomycin C day8
Aphidicolin day8
J
Symmetry ratio
Control day1
Control day8
Mitomycin C day8
Aphidicolin day8

Fig.2

A

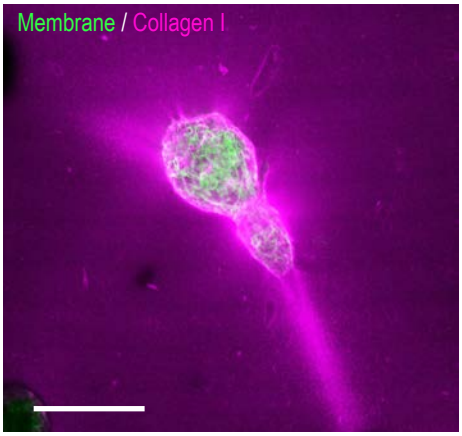

B

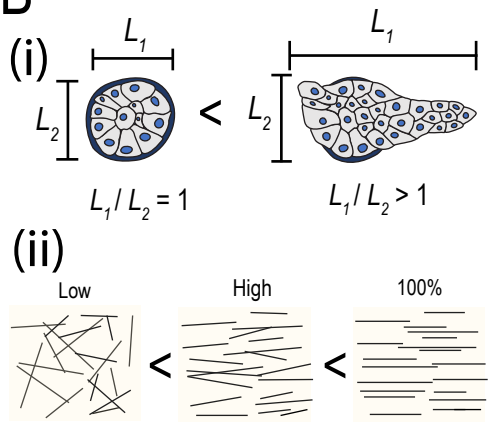

C

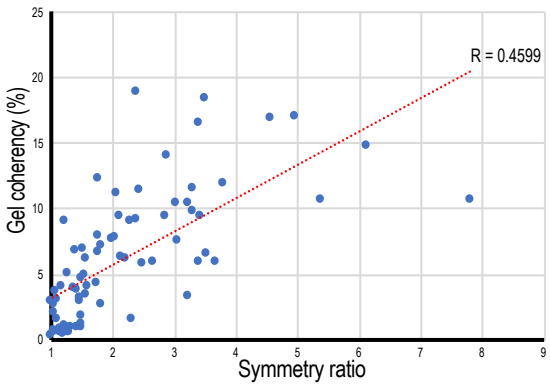

D

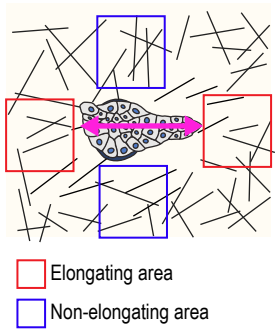

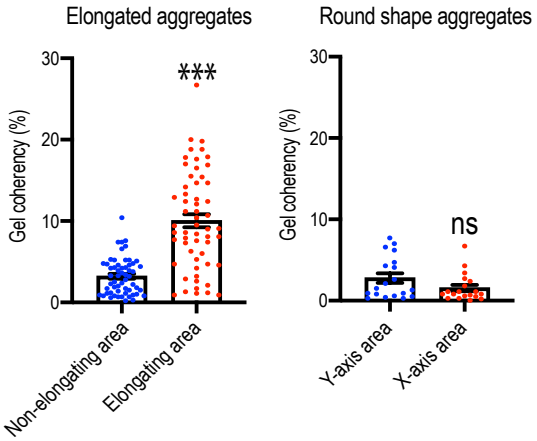

E

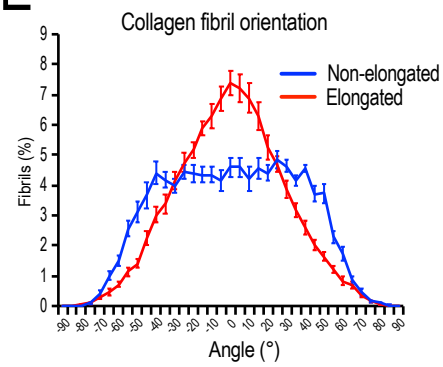

F

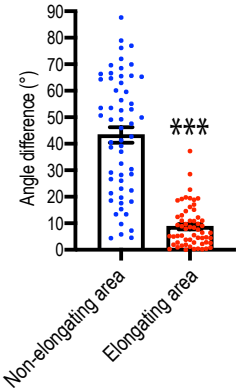

G

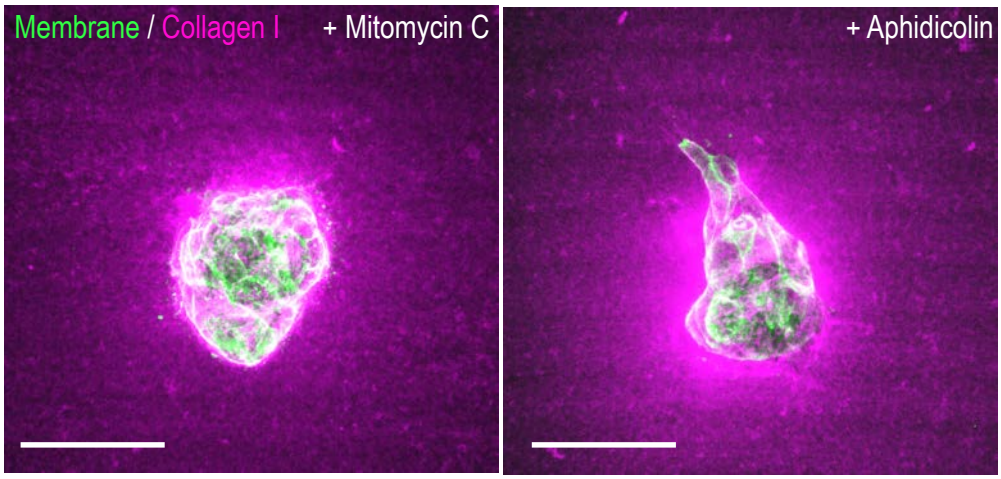

H

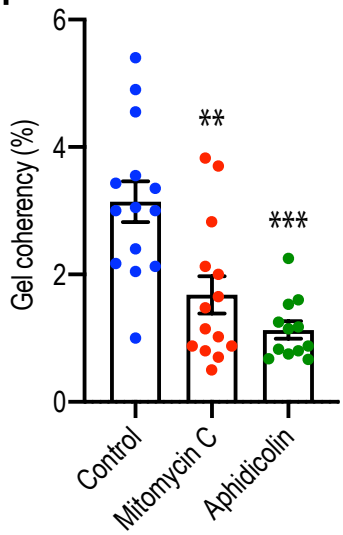

I

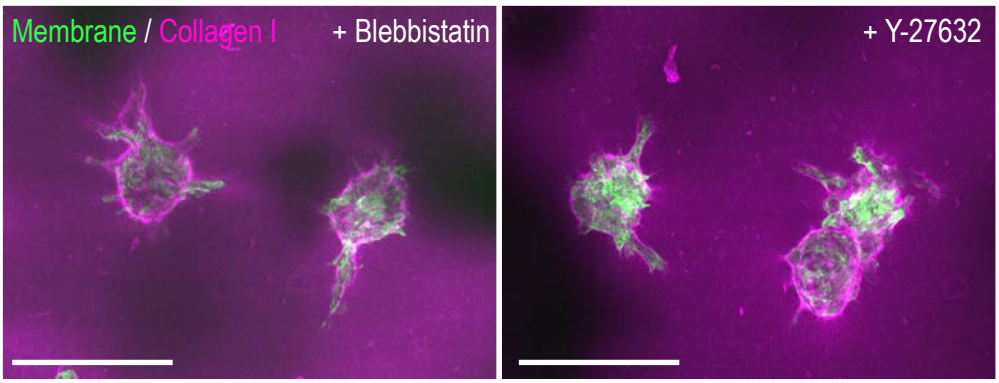

J

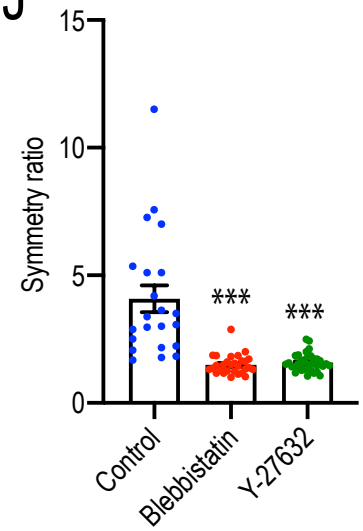

Fig. 3

A

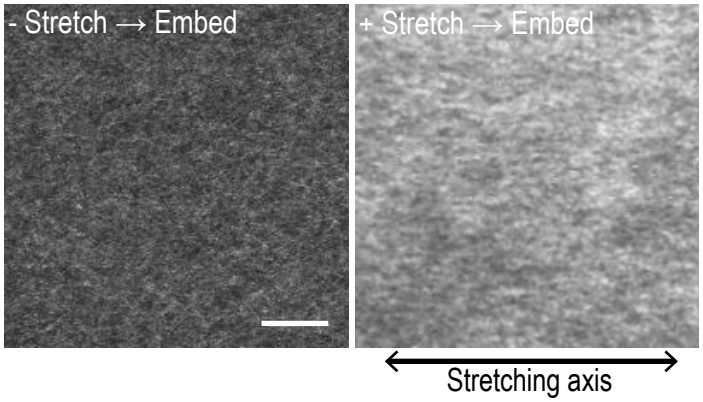

B

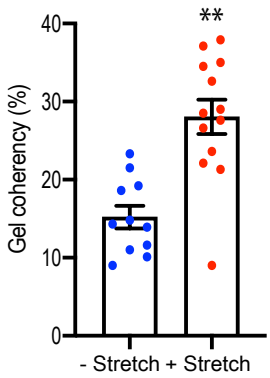

C

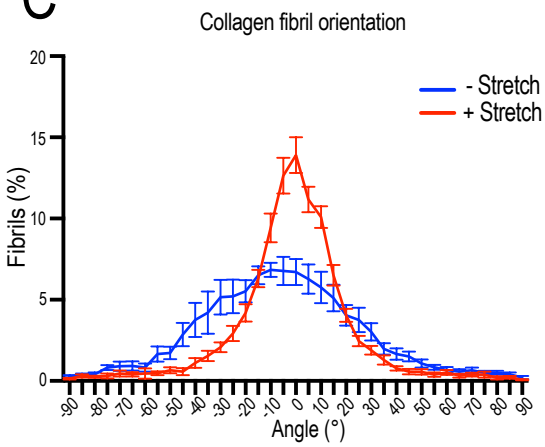

D

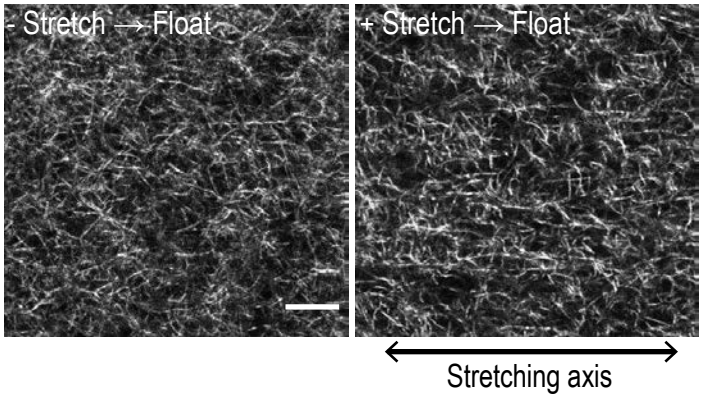

E

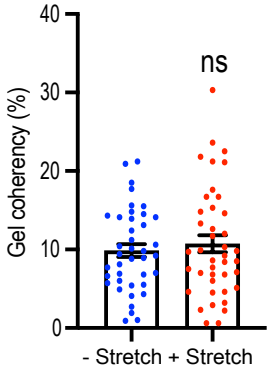

F

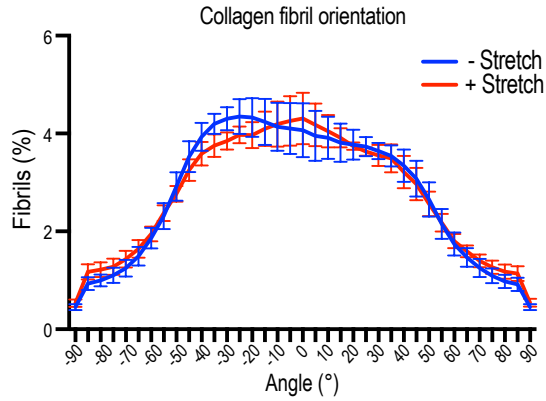

G

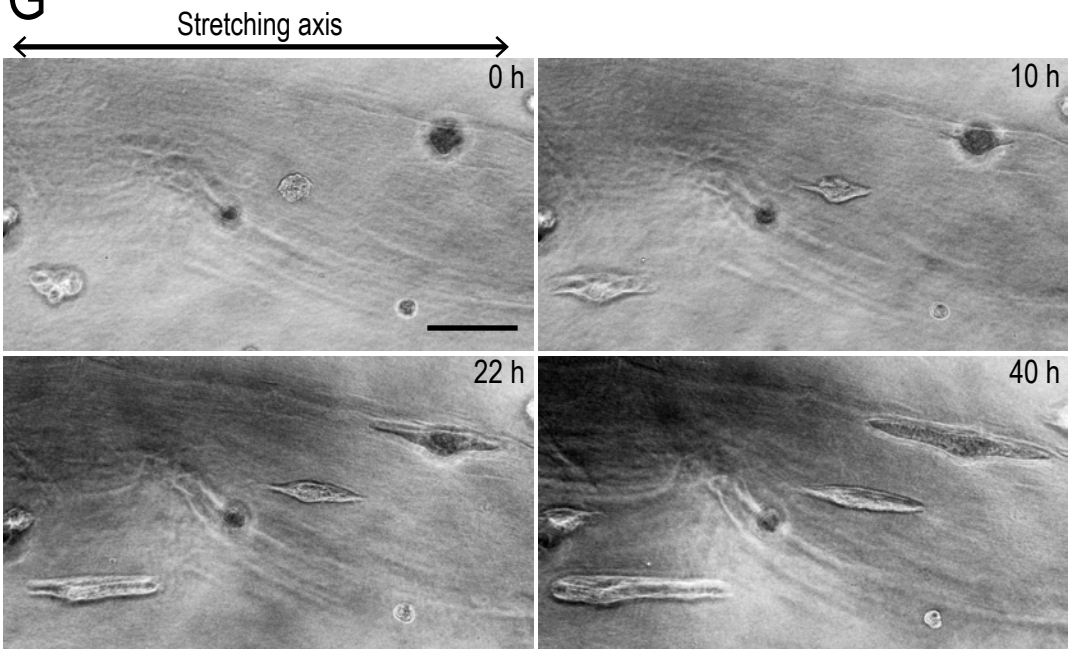

H

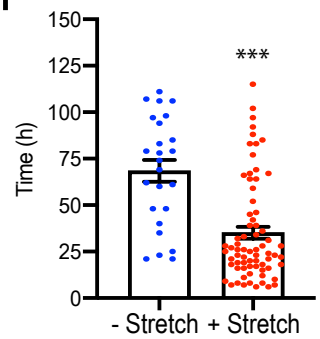

I

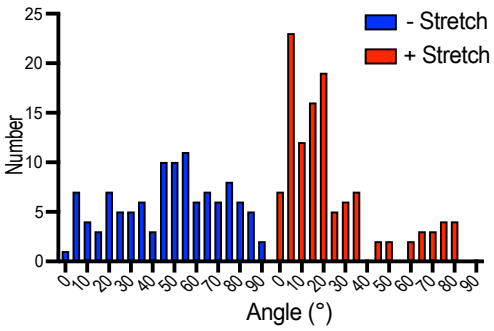

J

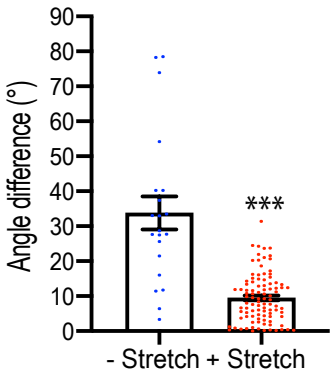

K

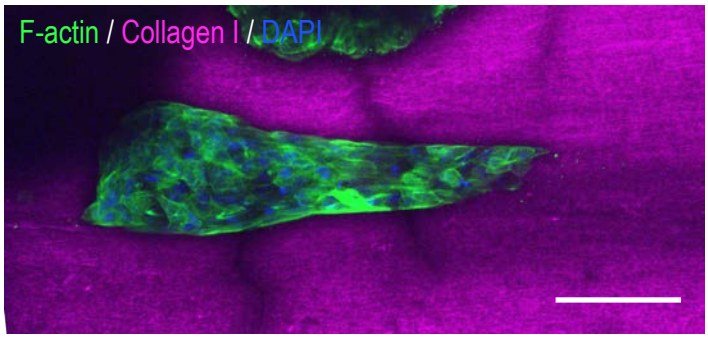

L

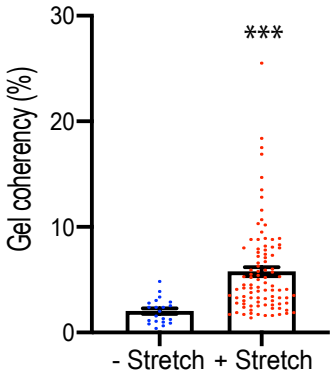

Fig. 4

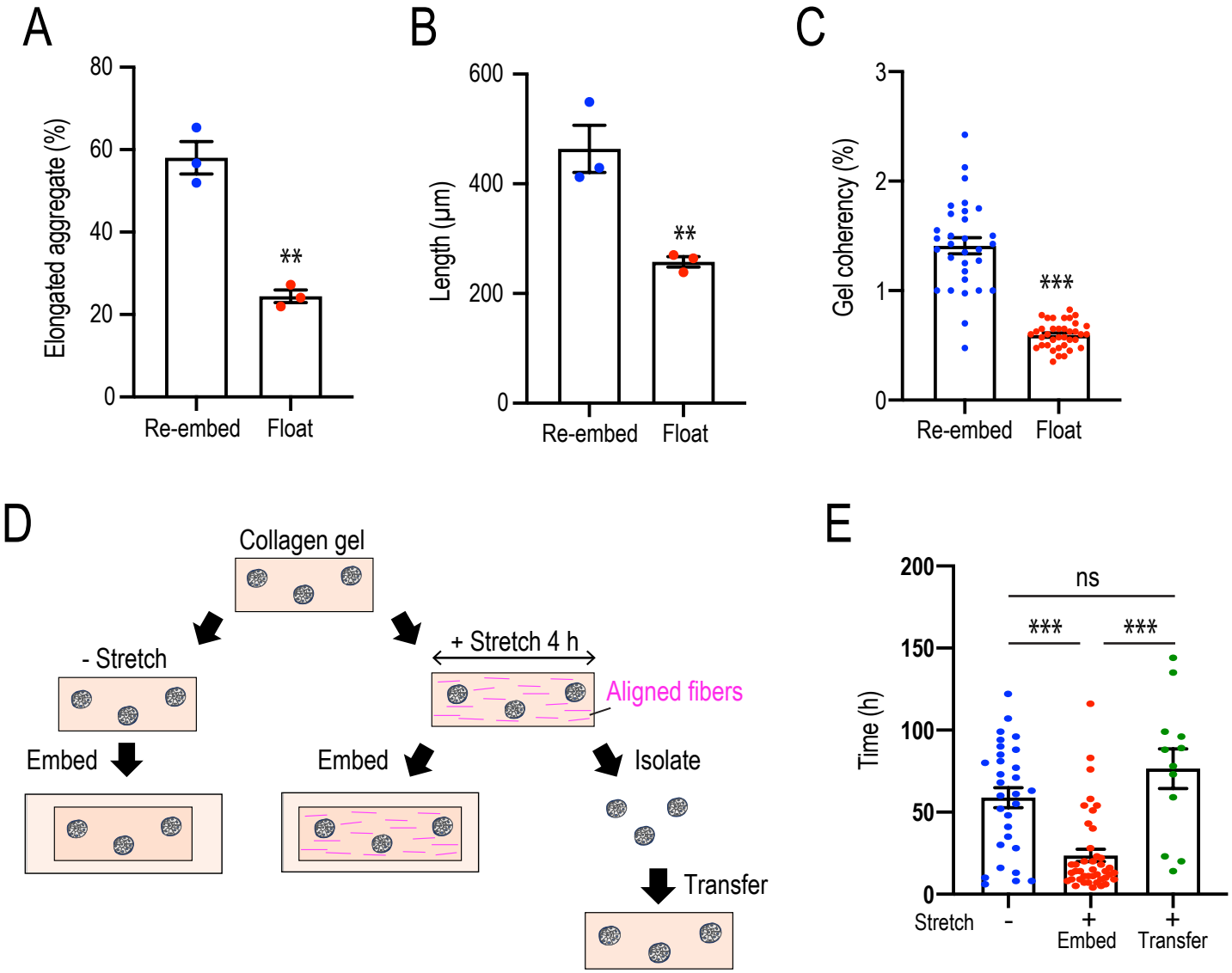
A
Elongated aggregate (%)
80
60
40
20
0
**
Re-embed
Float
B
Length (μm)
600
400
200
0
**
Re-embed
Float
C
Gel coherency (%)
3
2
1
0
***
Re-embed
Float
D
Collagen gel
- Stretch
Embed
+ Stretch 4 h
Aligned fibers
Embed
Isolate
Transfer
E
Time (h)
200
150
100
50
0
ns
***
***
Stretch
-
+
Embed
+
Transfer

Fig. 5

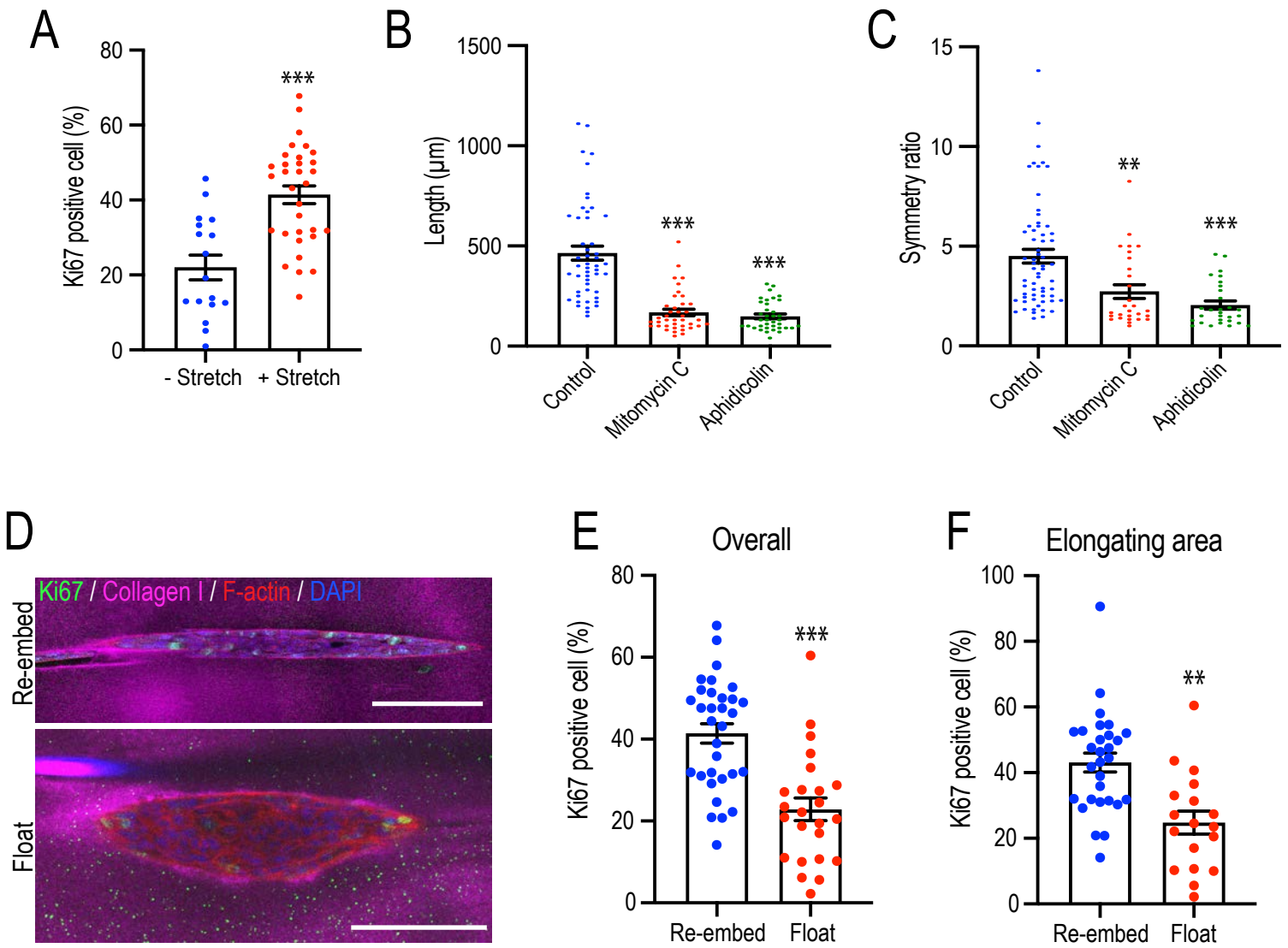
A
Ki67 positive cell (%)
80
60
40
20
0
***
- Stretch
+ Stretch
B
Length (μm)
1500
1000
500
0
***
***
Control
Mitomycin C
Aphidicolin
C
Symmetry ratio
15
10
5
0
**
***
Control
Mitomycin C
Aphidicolin
D
Ki67 / Collagen I / F-actin / DAPI
Re-embed
Float
E
Overall
Ki67 positive cell (%)
80
60
40
20
0
***
Re-embed
Float
F
Elongating area
Ki67 positive cell (%)
100
80
60
40
20
0
**
Re-embed
Float

Fig. 6

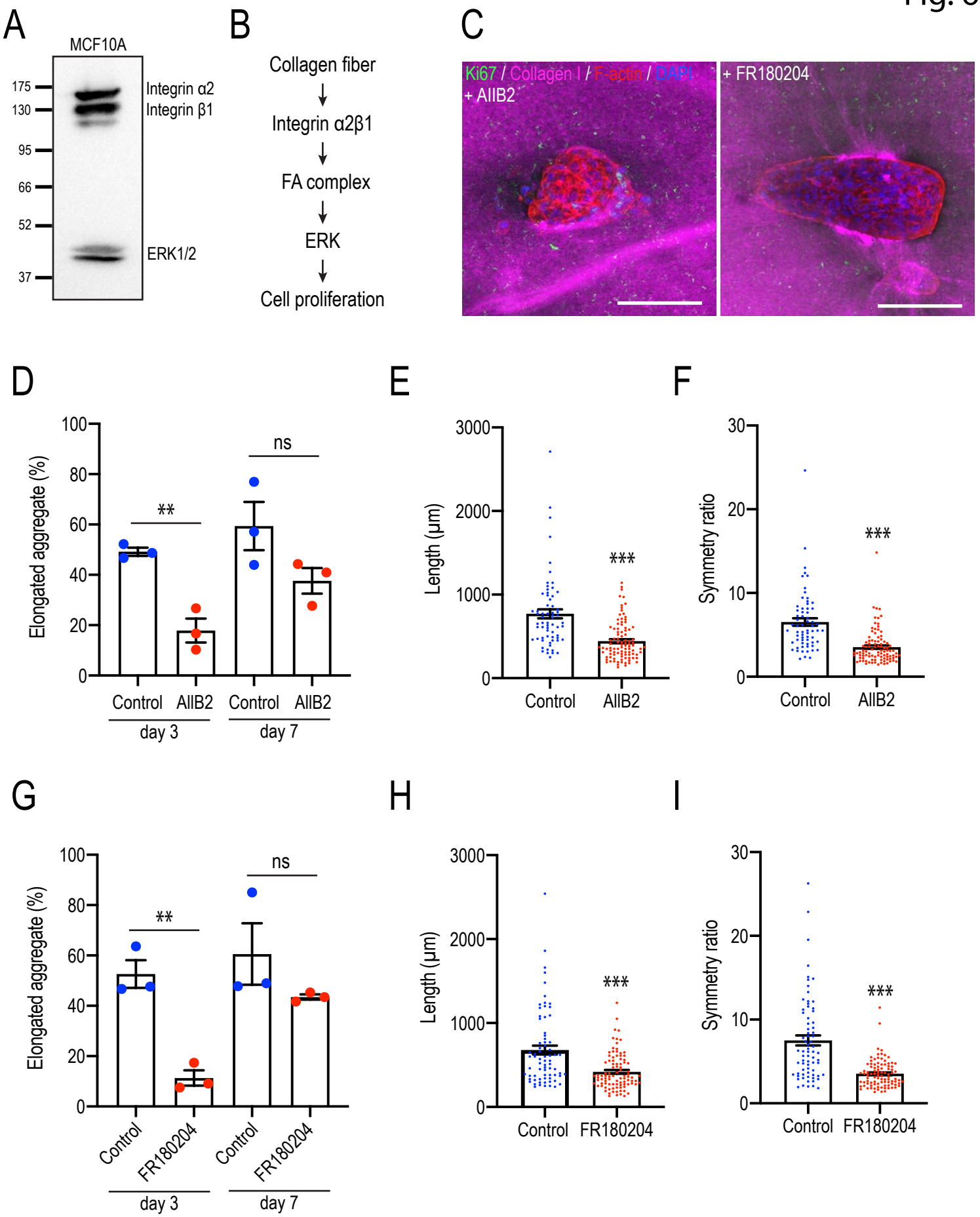
A
MCF10A
175
130
95
66
52
37
Integrin α2
Integrin β1
ERK1/2
B
Collagen fiber
Integrin α2β1
FA complex
ERK
Cell proliferation
C
Ki67 / Collagen I / F-actin / DAPI
+ AIIB2
+ FR180204
D
Elongated aggregate (%)
ns
**
Control
AIIB2
Control
AIIB2
day 3
day 7
E
Length (μm)
***
Control
AIIB2
F
Symmetry ratio
***
Control
AIIB2
G
Elongated aggregate (%)
ns
**
Control
FR180204
Control
FR180204
day 3
day 7
H
Length (μm)
***
Control
FR180204
I
Symmetry ratio
***
Control
FR180204

Fig.7

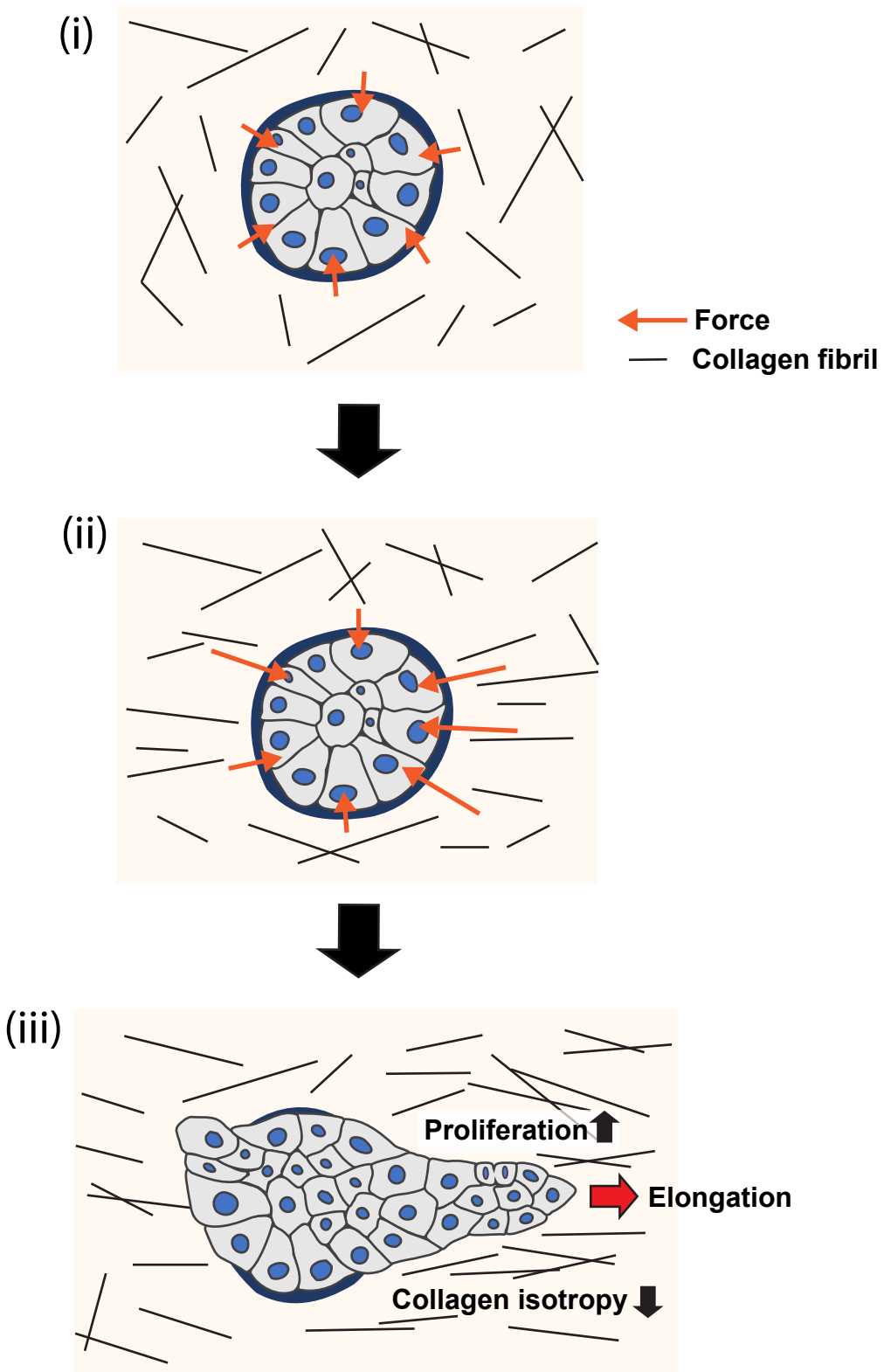
(i)
Force
Collagen fibril
(ii)
(iii)
Proliferation
Elongation
Collagen isotropy